atom coordinates in non-centrosymmetric isomorphs of proteins as revealed by Bricogne (1984). From (13*c*) and (14), it is evident that (13*a*), (15) and (17) are also obtained by using only a subset of observations composed of P_i^{obs} and the total backgrounds B_i^{obs}.

The fraction of $P_i^{obs} - P_i^{calc}$ which is attributed to the background intensity according to (15) increases with decreasing ratio of peak-to-background intensity. As expected, it reaches large values for very weak Bragg reflections. The covariance of P_i^{obs} and B_i^{obs} is normally a negative quantity. Thus, if $P_i^{calc} \gtrless P_i^{obs}$, then $B_i^{calc} \lessgtr B_i^{obs}$. In the following example, we assume that the variances of the observed intensities are derived from Poisson statistics, $s(Q_i) = Q_i^{obs}$, $s(L_i) = L_i^{obs}$, $s(H_i) = H_i^{obs}$ and $s(Q_iL_i) = s(Q_iH_i) = s(L_iH_i) = 0$. We also assume $l_i = h_i = 2$. In terms of the ratio of integrated intensity to total background $g_i = Q_i^{obs}/(l_iL_i^{obs} + h_iH_i^{obs})$, one obtains

$$B_i^{obs} - B_i^{calc} = -[2/(g_i+2)](P_i^{obs} - P_i^{calc}).$$

The fractions of $P_i^{obs} - P_i^{calc}$ attributed to the background are 2, 17, 67 and 100% for $g_i = 100$, 10, 1 and 0, respectively. Negative net intensities imply $g_i < 1$.

The model for the background intensities that we have used might be described as the *independent background* model, in which each and every reflection has its own independent variable parameters quantifying both the low-and high-angle backgrounds. A large number of variable parameters results but the total background is readily estimated using (15). Alternatively, the background might be represented by some more elaborate model in terms of a few variable global parameters. There is a risk of introducing additional modelling error, but the number of variables is considerably reduced. Once a suitable model has been found, it is easily introduced in (5) and the setting up of the corresponding normal equations is straightforward. However, we note that the structural parameters ν_m and the parameters describing the background are correlated and should be refined together. We do not recommend fitting the background intensities to their observed values first and then subtracting the resulting calculated backgrounds from the integrated scan intensities to obtain net intensities since the errors of such net intensities are correlated.

References

BRICOGNE, G. (1984). In *Methods and Applications in Crystallographic Computing*, edited by S. R. HALL & T. ASHIDA, pp. 141-151. Oxford: Clarendon Press.

FRENCH, S. & WILSON, K. (1978). *Acta Cryst.* A**34**, 517-525.

HIRSHFELD, F. L. & RABINOVICH, D. (1973). *Acta Cryst.* A**29**, 510-513.

SHORT COMMUNICATIONS

Contributions intended for publication under this heading should be expressly so marked; they should not exceed about 1000 *words; they should be forwarded in the usual way to the appropriate Co-editor; they will be published as speedily as possible.*

Acta Cryst. (1991). A**47**, 137-139

A computational method for obtaining stationary solutions in RHEED and REM.

By Y. MA,* *Materials Research Center, Northwestern University, Evanston, IL* 60208, *USA*

(*Received* 17 *January* 1990; *accepted* 4 *September* 1990)

Abstract

The application of the multislice approach of Cowley & Moodie [*Acta Cryst.* (1959), **12**, 353-359] to reflection high-energy electron diffraction (RHEED) may suffer from edge effects which continuously degrade the edge of the unit cell and prevent stationary solutions from being obtained for RHEED. The reason for this is that it is difficult to simulate a tilted infinite plane wave for the beam geometry of RHEED in a finite unit cell. It is shown that this can be done with a simple edge-patching method. It is then possible to obtain an infinitely convergent stationary solution for an arbitrary surface in RHEED within a finite unit cell.

The arrangement of the artificial supercell for the simulation of RHEED patterns (Peng & Cowley, 1986) using the Cowley-Moodie multislice approach (Cowley & Moodie, 1959) is similar to that used for the simulation of profile images in high-resolution electron microscopy (HREM). The unit cell is split into two parts, the first is a vacuum and the second contains atoms that comprise the crystal surface. The difference is that, for profile imaging, the incident plane wave is not tilted as much and illuminates the whole unit cell, while for the simulation of RHEED it is more tilted and only illuminates the vacuum part of the unit cell. If we have a propagator with a fixed slice thickness and an empty phase grating, the result of each iteration is simply to add a constant phase term to the initial incident wave function, which resulted from the convolution of the incident-wave function with a fixed propagation function. This phase term can be easily calculated either analytically or numerically. For the simulation of RHEED patterns, the phase grating in the edge area of the vacuum part of each unit cell is empty since the surface potential exponentially decays to near zero into the vacuum. Therefore, in this edge

* Present address: Department of Physics, University of Oslo, PO Box 1048 Blindern, 0316 Oslo 3, Norway.

0108-7673/91/020137-03$03.00

area, the multislice iteration does nothing more than continuously introduce a constant phase increment to the initially tilted incident plane wave. However, since the incident plane wave is artificially cut off at the edge of the unit cell near *A* in Fig. 1(i) because of the limited cell size (and also tilted), the edge will move towards the crystal surface and degrade the solution before it becomes stationary. The boundary of the artificial computational superlattice thus becomes the source of an unwanted set of Fresnel fringes (edge movement), which encroaches on the crystal. Theoretically, one can always make the unit cell large enough to delay this deterioration process, but this is impractical in many circumstances, especially when simulating surface imperfections. It should be noted that this edge-deterioration process is not the result of imposing Bloch-like periodic boundary conditions in the multislice

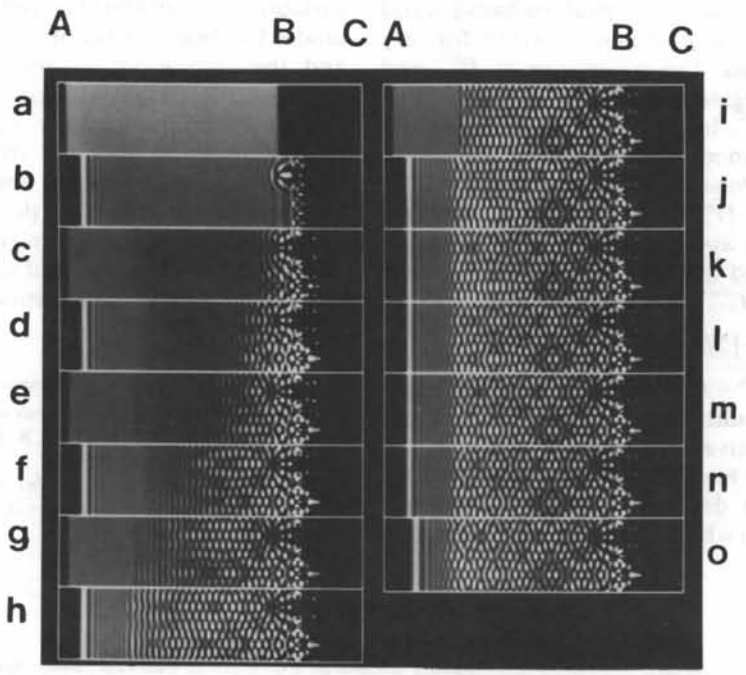

(i)

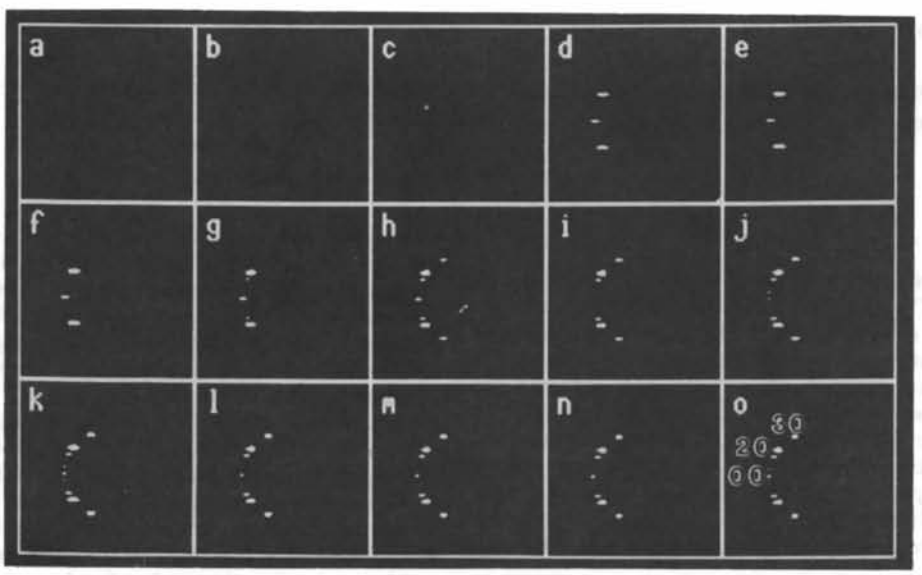

(ii)

Fig. 1. (i) Wave fields calculated for the 2×1 Au(001) surface using the new method. The calculation is for 100 keV incident electrons, 30 mrad incident angle and 10% absorption. The picture shows the electron intensity distribution on a plane normal to the beam both outside (from *A* to *B*) and inside (from *B* to *C*) the crystal. The series of output of slice numbers is 1, 100, 200, 300, 400, 500, 600, 700, 800, 1100, 1300, 1500, 1700, 2050. The page normal is [010]. (ii) Simulated RHEED patterns corresponding to (i).

approach, the effects of which become trivial when absorption and a Gaussian smoothed incident plane wave are introduced, since both damp the wave field near two ends of each slice to zero, so that the periodic boundary interference becomes negligible.

For the edge area of the vacuum part of each unit cell, each multislice iteration is equivalent to adding a constant phase term to the incident tilted plane wave in the same area. We may therefore always repair this edge area by replacing it with the corresponding edge area of a tilted incident plane wave as long as the wave function in this area is multiplied by a proper phase term which can be easily calculated. Thus the small limited patched edge area in fact plays the role of an infinite plane-wave source which is crucial for obtaining a stationary solution for RHEED. It should be pointed out that it is not necessary to repair the deteriorated edge often because the moving edge seriously deteriorates the solution only after a certain number of iterations. Therefore, the computation time does not increase significantly due to the 'repairing'. The rate of deterioration of the edge depends primarily upon two parameters, the incident angle (θ_0) and the slice thickness (Δz), and the frequency of repairing can be made self-adjustable in the program.

Fig. 1(i) shows the results calculated for the 2×1 missing row reconstruction on the Au(001) surface. All calculation conditions are the same as those for Fig. 2(i) in our previous paper (Ma & Marks, 1990), except that the edge-patching method is used and 2050 iterations are calculated here. The surface is set at B and 3/4 of each slice on the left (from A to B) contains the vacuum wave and 1/4 of each slice on the right (from B to C) contains the crystal wave. The beam direction is along [010]. The calculation thickness is much thicker than that previously used, up to 2075·5 Å. It is infinite theoretically. The last four slices in Fig. 1(i) demonstrate that the stationary solution for the 2×1 Au(001) surface has been obtained. The patched edge area only shows the tilted plane-wave component when the stationary solution gradually forms in the non-patched-edge area. Since the wave front of the Bragg reflected waves always moves away from the crystal, the discontinuity between these two areas will not affect the final solution as long as the continuity of the incident-plane-wave components in these two areas is well preserved. Fig. 1(ii) shows the RHEED patterns corresponding to Fig. 1(i). They are Fourier transforms of the vacuum waves excluding the patched area in the slices in Fig. 1(i). The incident beam has been cut off. The reconstruction spots and spots corresponding to the double period on the 2×1 Au(001) surface (03) have emerged in the stationary solution shown in the last four patterns.

This work was supported by the National Science Foundation, Grant no. DMR 85-20280 and DMR 87-17376. The author is very grateful for many useful discussions with Professor L. D. Marks about this work.

References

COWLEY, J. M. & MOODIE, A. F. (1959). *Acta Cryst.* **12**, 353-359.
MA, Y. & MARKS, L. D. (1990). *Acta Cryst.* A**46**, 594-606.
PENG, L. M. & COWLEY, J. M. (1986). *Acta Cryst.* A**42**, 545-552.

Acta Cryst. (1991). A**47**, 139-142

Observation of nonprojective moiré fringe patterns produced with an X-ray interferometer.

By J. YOSHIMURA, *Institute of Inorganic Synthesis, Faculty of Engineering, Yamanashi University, Kofu* 400, *Japan*

(*Received* 6 *December* 1989; *accepted* 12 *September* 1990)

Abstract

Moiré fringes produced with an X-ray interferometer have been found to give an extraordinary nonprojectiveness, an oscillatory change of the fringe position along the beam paths of the transmitted and the Bragg reflected waves behind the interferometer. Densitometric measurements of the moiré fringes showed that, along with the fringe position, the fringe profile changes in an unusual manner along the beam paths. This nonprojectiveness is presumably of the same nature as that observed for moiré fringes produced with a bicrystal [Yoshimura (1989). *J. Phys. Soc. Jpn*, **58**, 1283-1295].

In recent papers (Yoshimura, 1987, 1989), it has been shown that X-ray moiré fringes observed with a bicrystal specimen are not exactly the projection of the intensity distribution of the wave field on the exit surface of the crystal, but do oscillate along the beam paths behind the crystal. This nonprojectiveness of moiré fringes is inexplicable by the current theory of moiré fringes (*cf.* Yoshimura, 1989) and therefore is of interest. In this paper we report a similar fringe oscillation observed for moiré fringes produced with an X-ray interferometer. The present moiré fringes are nearly a parallel moiré pattern while the previous ones were nearly a rotation moiré pattern.

The experimental set-up was basically the same as before [see Fig. 1 in Yoshimura (1989)]. X-ray topographs of moiré patterns were taken with a double-crystal arrangement in the parallel setting for Si 220 reflection with Mo $K\alpha$ radiation. An asymmetrically cut collimator crystal was used so as to make the angular spread of the incident beam on the specimen 0·45″. A standard *LLL*-type X-ray interferometer (Bonse & Hart, 1965), about 26 mm long and 25 mm wide, was mounted on the specimen position instead of the bicrystal. The surfaces of the three components of the X-ray interferometer were parallel to (111), and their thicknesses were 0·8 mm. To produce moiré patterns, a point on the top of the analyzer wafer was locally heated. Very thin Pt wires stretched in a frame were placed between the specimen and X-ray films so that their shadow images gave a standard for position and/or orientation on the topographs. Moiré patterns were recorded simultaneously on three to seven X-ray films placed at different distances

0108-7673/91/020139-03$03.00